

Quantum Detection of Sequency-Band Structure

Alok Shukla ^{*1} and Prakash Vedula²

¹School of Arts and Sciences, Ahmedabad University, India

¹alok.shukla@ahduni.edu.in

²School of Aerospace and Mechanical Engineering, University of Oklahoma, USA

²pvedula@ou.edu

Abstract

We present a quantum algorithm for estimating the amplitude content of user-specified sequency bands in quantum-encoded signals. The method employs a sequency-ordered Quantum Walsh–Hadamard Transform (QWHT), a comparator-based oracle that coherently marks basis states within an arbitrary sequency range, and Quantum Amplitude Estimation (QAE) to estimate the total probability mass in the selected band. This enables the detection of structured signal components, including both high- and low-sequency features, as well as the identification of rapid sign-change behavior associated with noise or anomalies. The proposed method can be embedded as a module within a larger quantum algorithm; in this setting, both the input and output remain fully quantum, enabling seamless integration with upstream and downstream quantum operations. We show that the sequency-ordered QWHT can be implemented with circuit depth $O(\log_2 N)$ (equivalently $O(n)$ for $N = 2^n$) when acting on an amplitude-encoded quantum state, whereas computing the full Walsh–Hadamard spectrum of an explicit length- N classical signal requires $O(N \log_2 N)$ operations via the fast Walsh–Hadamard transform. This results in an exponential quantum advantage when the QWHT is used as a modular block within a larger quantum algorithm, relative to classical fast Walsh–Hadamard transform-based approaches operating on explicit data. From an application perspective, the proposed sequency band-energy estimation may be interpreted as a structure-based anomaly indicator, enabling the detection of unexpected high-sequency components relative to a nominal low-sequency signal class. The algorithm is applicable to quantum-enhanced signal processing tasks such as zero-crossing analysis, band-limited noise estimation, and feature extraction in the Walsh basis.

1 Introduction

In recent years, quantum computing has matured into a powerful algorithmic framework, supported by a growing body of quantum algorithms that demonstrate provable advantages over classical methods for structured computational tasks [1]. This includes Deutsch–Jozsa algorithm [2], the Bernstein–Vazirani algorithm [3] and its probabilistic generalization [4], Simon’s algorithm [5], quantum search algorithm [6,7], quantum Fourier transform, quantum phase estimation [8–11], quantum amplitude estimation [10,12,13] and Shor’s polynomial-time algorithms for integer factorization and discrete logarithms and its variants

^{*}Corresponding author.

[14, 15]. Quantum algorithms have since been developed for a wide range of scientific and engineering applications, including trajectory optimization [16], the solution of large-scale linear systems [17], linear and nonlinear differential equations [18–20], and digital image, signal processing and spectral analysis [21–24], efficient state preparation [25–28], quantum optimal control [29] and numerical integration [30–32]. This paper contributes to this broader landscape by developing a fully quantum, sequency-resolved noise-detection primitive based on the sequency-ordered Quantum Walsh-Hadamard Transform (QWHT) and amplitude estimation.

Taken together, these developments underscore the increasing relevance of quantum algorithms for practical computational tasks, extending well beyond purely complexity-theoretic demonstrations.

Spectral analysis plays a central role in many scientific and engineering disciplines, including signal processing, image analysis, communications, and biomedical diagnostics. Detecting the energy content in specific frequency or sequency bands is critical for identifying structured noise patterns, abrupt transitions, or meaningful signal features. Classical approaches typically rely on transforms such as the Discrete Fourier Transform (DFT) or the Walsh-Hadamard Transform (WHT), followed by band selection and energy estimation. The Walsh basis, particularly in its sequency-ordered form, is closely tied to the number of sign changes (or zero-crossings) in basis functions, making it a natural tool for such analysis.

Quantum computing provides new tools to address these tasks more efficiently in high-dimensional settings. In this work, we propose a quantum algorithm that performs band-specific sequency analysis by leveraging the sequency-ordered Quantum Walsh-Hadamard Transform (QWHT), a custom comparator-based oracle to select basis states in a target sequency band, and amplitude estimation to quantify their contribution. Unlike prior approaches limited to global spectral properties or requiring classical postprocessing, our method enables fully quantum estimation of amplitudes in arbitrary Walsh bands.

A classical technique for assessing signal frequency content is the count of zero-crossings in the signal. Zero-crossings, corresponding to sign changes in sampled data, are a well-known heuristic for detecting high-frequency behavior. Moreover, the Walsh-Hadamard Transform (WHT) in its sequency-ordered form, provides a direct spectral basis in which high-frequency components correspond to high-sequency indices. Quantum computing offers the possibility of analyzing signal structure more efficiently in high-dimensional spaces.

Main Contributions

In this paper, we present a quantum algorithm that addresses the zero-crossing detection problem from a fully quantum perspective. First, we implement the Quantum Walsh-Hadamard Transform in sequency order using a low-depth quantum circuit that avoids classical postprocessing. We then design a comparator-based quantum oracle that efficiently flags those basis states whose sequency indices lie within a user-specified high-frequency band. This is followed by the application of Quantum Amplitude Estimation, which allows us to estimate the probability mass associated with the flagged sequency components. Crucially, this estimated amplitude is shown to be directly related to the number of zero-crossings in the original signal. As a result, the entire procedure constitutes a new quantum algorithm for zero-crossing detection that is both rigorous and resource-efficient.

The proposed algorithm is broadly applicable to several quantum-enhanced tasks, including signal and image processing, biomedical signal analysis (such as EEG and ECG), spectral sparsity detection in compressed sensing, and feature selection in quantum machine learning pipelines. We support our theoretical development with explicit circuit constructions, oracle design details, and numerical simulations on small

quantum systems. Altogether, our results demonstrate how spectral properties of classical signals can be extracted efficiently in a quantum computational framework.

In this work, we also present a quantum circuit for performing the Walsh–Hadamard transforms in sequency ordering. We note that usually the Walsh–Hadamard transform in natural order appears in quantum algorithms (for example, Deutsch–Jozsa algorithm [2], Bernstein–Vazirani algorithm [3], Simon’s algorithm [5], Grover’s algorithm [6], Shor’s Algorithm [14], etc.), often to get a uniform superposition of quantum states at the beginning of the quantum algorithm. The Walsh–Hadamard transform in natural order and the associated Walsh basis functions in natural order have also been used in the solution of non-linear ordinary differential equations [20]. On the other hand, the Walsh basis functions and the Walsh–Hadamard transforms in sequency ordering have found applications in several domains in engineering, for example, digital image and signal processing [33, 34], cryptography [35], solution of non-linear ordinary differential equations and partial differential equations [36–40]. In image processing applications, it is often desired to use Walsh basis functions in sequency ordering because of better energy compaction properties. For instance, the hybrid classical-quantum algorithm approach for image processing discussed in [21] uses the Walsh–Hadamard transforms in sequency ordering. We note that in [41], the quantum Walsh–Hadamard transform is performed in natural order, followed by classical computations to obtain the transforms in sequency ordering. In this and other applications wherein the Walsh–Hadamard transform in sequency ordering is needed, it is desirable to have a quantum circuit to compute the Walsh–Hadamard transforms directly in sequency ordering.

This article is organized as follows. Section 1.1 introduces the notation used throughout the paper. In Section 2, we formalize the zero-crossing counting problem. Section 3 presents a quantum circuit for implementing the Walsh–Hadamard transform in sequency ordering. Numerical simulation results validating the proposed framework are reported in Section 5. Finally, Section 6 concludes the paper and discusses future directions.

1.1 Notation

Before proceeding further, we define some convenient notations used in the rest of the paper.

- \oplus : $x \oplus y$ will denote $x + y \pmod{2}$.
- $s \cdot x$: For $s = s_{n-1}s_{n-2}\dots s_1s_0$ and $x = x_{n-1}x_{n-2}\dots x_1x_0$ with $s_i, x_i \in \{0, 1\}$, $s \cdot x$ will denote the bit-wise dot product of s and x modulo 2, i.e., $s \cdot x := s_0x_0 + s_1x_1 + \dots + s_{n-1}x_{n-1} \pmod{2}$.
- $s(m)$: For $s = s_{n-1}s_{n-2}\dots s_2s_1s_0$ and $1 \leq m \leq n$, $s(m)$ denotes the string formed by keeping only the m least significant bits of s , i.e., $s(m) = s_{m-1}s_{m-2}\dots s_2s_1s_0$.
- On a few occasions, by abuse of notations, a non-negative integer s , such that $s = \sum_{j=0}^{n-1} s_j 2^j$, will be used to represent the n -bit string $s_{n-1}s_{n-2}\dots s_2s_1s_0$.

2 Zero-crossings counting problem

Let the function $F: \{0, 1\}^n \rightarrow \{1, -1\}$ be defined as $F(x) = (-1)^{f(x)}$, where $f(x) = s \cdot x$ for some fixed string $s \in \{0, 1\}^n$. The number of zero-crossings (i.e., sign changes) for the sequence

$$\mathcal{S} = (F(0), F(1), F(2), \dots, F(2^n - 1)) \quad (2.1)$$

Secret string, s	Sequence $\mathcal{S} = (F(k))_{k=0}^7$	Number of zero-crossings (sign changes)
000	(1, 1, 1, 1, 1, 1, 1, 1)	0
001	(1, -1, 1, -1, 1, -1, 1, -1)	7
010	(1, 1, -1, -1, 1, 1, -1, -1)	3
011	(1, -1, -1, 1, 1, -1, -1, 1)	4
100	(1, 1, 1, 1, -1, -1, -1, -1)	1
101	(1, -1, 1, -1, -1, 1, -1, 1)	6
110	(1, 1, -1, -1, -1, -1, 1, 1)	2
111	(1, -1, -1, 1, -1, 1, 1, -1)	5

Table 1: The table shows the number of zero-crossings (sign changes) for the sequence $(F(k))_{k=0}^7$, with $F(k) = (-1)^{s \cdot k}$, for $s = 000, 001, \dots, 111$.

is defined as

$$\frac{1}{2} \sum_{k=0}^{N-2} |F(k+1) - F(k)| = \frac{1}{2} \sum_{k=0}^{N-2} |(-1)^{s \cdot (k+1)} - (-1)^{s \cdot k}|, \quad (2.2)$$

where $N = 2^n$. The numbers of zero-crossings for sequences associated with different secret strings (for $n = 3$) are listed in Table 1. The computation of the number of zero-crossings for the sequence associated with the secret string $s = 101$ is illustrated in Ex. 2.0.1.

Example 2.0.1. Let $n = 3$ and $s = 101$ (or equivalently $s = 5$). Clearly,

$$\begin{aligned} s \cdot 0 &= (101) \cdot (000) = (1 \times 0) \oplus (0 \times 0) \oplus (1 \times 0) = 0, \\ s \cdot 1 &= (101) \cdot (001) = (1 \times 0) \oplus (0 \times 0) \oplus (1 \times 1) = 1, \\ s \cdot 2 &= (101) \cdot (010) = (1 \times 0) \oplus (0 \times 1) \oplus (1 \times 0) = 0, \\ &\dots \\ s \cdot 7 &= (101) \cdot (111) = (1 \times 1) \oplus (0 \times 1) \oplus (1 \times 1) = 0. \end{aligned}$$

Then

$$\mathcal{S} = \left((-1)^{s \cdot 0}, (-1)^{s \cdot 1}, (-1)^{s \cdot 2}, \dots, (-1)^{s \cdot 7} \right) = (1, -1, 1, -1, -1, 1, -1, 1).$$

Let $N = 2^n = 8$. The number of zero-crossings of the sequence \mathcal{S} is given by

$$\frac{1}{2} \sum_{k=0}^{N-2} |(-1)^{s \cdot (k+1)} - (-1)^{s \cdot k}| = \frac{1}{2} (|1 - 1| + |1 - (-1)| + |1 - 1| + |1 - (-1)| + |1 - (-1)| + |1 - 1| + |1 - (-1)|) = 6.$$

2.1 A technical lemma

Let

$$g = \sum_{j=0}^{n-1} g_j 2^j, \quad (2.3)$$

and the bits of g are given by

$$\begin{aligned} g_{n-1} &= s_0, \\ g_{n-2} &= s_0 \oplus s_1, \\ &\dots \end{aligned}$$

$$g_1 = s_0 \oplus s_1 \oplus s_2 \oplus \dots \oplus s_{n-2},$$

$$g_0 = s_0 \oplus s_1 \oplus s_2 \oplus \dots \oplus s_{n-2} \oplus s_{n-1}.$$

It means,

$$g_{n-1} = s_0, \quad \text{and} \quad g_k = s_0 \oplus s_1 \oplus \dots \oplus s_{n-1-k}, \quad \text{for } k = n-2 \text{ to } 0. \quad (2.4)$$

Finally, all the qubits (except the ancilla qubit) are measured and stored in a classical register. The classical bits resulting from these measurements are labeled g_0 to g_{n-1} in Fig. 3. Indeed, g is number of zero-crossings of the sequence \mathcal{S} (as defined in Eq. (2.1)). We recall that, the number of zero-crossings of the sequence \mathcal{S} (as defined in Eq. (2.1)) is given by

$$\frac{1}{2} \sum_{k=0}^{N-2} |(-1)^{s \cdot (k+1)} - (-1)^{s \cdot k}|,$$

as noted in Eq. (2.2). It follows from Corollary 2.1.2 that $g = Z_n(s) = \frac{1}{2} \sum_{k=0}^{N-2} |(-1)^{s \cdot (k+1)} - (-1)^{s \cdot k}|$ is the number of zero-crossings of the sequence \mathcal{S} that we wanted to determine.

In this section, we will prove Lemma 2.1.1 and its corollary (Corollary 2.1.2) to show that $g = \sum_{j=0}^{n-1} g_j 2^j$ (see Eq. (2.3) and Eq. (2.4)) gives the number of zero-crossings in the sequence \mathcal{S} given by

$$\mathcal{S} = (F(0), F(1), F(2), \dots, F(2^n - 1)),$$

with $F(x) = (-1)^{f(x)}$ and $f(x) = s \cdot x$ (ref. Eq. (2.1)).

Lemma 2.1.1. *For an integer m with $1 < m \leq n$, and for $x = x_{n-1} x_{n-2} \dots x_1 x_0$ (or equivalently, x with a decimal representation $x = \sum_{j=0}^{m-1} x_j 2^j$), with $x_j \in \{0, 1\}$, define $Z_m(x)$ as*

$$Z_m(x) := \frac{1}{2} \sum_{k=0}^{2^m-2} |(-1)^{x \cdot (k+1)} - (-1)^{x \cdot k}|. \quad (2.5)$$

Then, we have

$$Z_m(s(m)) = 2Z_{m-1}(s(m-1)) + (s_0 \oplus s_1 \oplus s_2 \oplus \dots \oplus s_{m-1}). \quad (2.6)$$

Here $s(m) = s_{m-1} s_{m-2} \dots s_1 s_0$ and $s_0 \oplus s_1 \oplus s_2 \oplus \dots \oplus s_{m-1} = (s_0 + s_1 + s_2 + \dots + s_{m-1}) \pmod{2}$. (ref. Sec. 1.1).

Proof. Let $M = 2^m$. We put $x = s(m)$ and split the summation on the right side of Eq. (2.5) into three different parts as follows.

$$\begin{aligned} Z_m(s(m)) &= \frac{1}{2} \left(\sum_{k=0}^{\frac{M}{2}-2} |(-1)^{s(m) \cdot (k+1)} - (-1)^{s(m) \cdot k}| \right) + \frac{1}{2} |(-1)^{s(m) \cdot (\frac{M}{2})} - (-1)^{s(m) \cdot (\frac{M}{2}-1)}| + \frac{1}{2} \sum_{k=\frac{M}{2}}^{M-2} |(-1)^{s(m) \cdot (k+1)} - (-1)^{s(m) \cdot k}|. \end{aligned} \quad (2.7)$$

We note that $\frac{M}{2} = 2^{m-1}$ represents the m -bit string $10\dots0$. Therefore, $s(m) \cdot \left(\frac{M}{2}\right) = s_{m-1}$. Similarly, $\frac{M}{2} - 1 = 2^{m-1} - 1$ represents the m -bit string $011\dots1$, hence $s(m) \cdot \left(\frac{M}{2} - 1\right) = s_0 \oplus s_1 \oplus s_2 \oplus \dots \oplus s_{m-2}$. Therefore, the middle term in the above summation reduces to

$$\frac{1}{2} |(-1)^{s(m) \cdot (\frac{M}{2})} - (-1)^{s(m) \cdot (\frac{M}{2}-1)}| = \frac{1}{2} |(-1)^{s_{m-1}} - (-1)^{s_0 \oplus s_1 \oplus \dots \oplus s_{m-2}}|$$

$$= s_0 \oplus s_1 \oplus s_2 \oplus \dots \oplus s_{m-1}. \quad (2.8)$$

Next we show that the last and the first terms are equal.

$$\begin{aligned} \frac{1}{2} \sum_{k=\frac{M}{2}}^{M-2} |(-1)^{s(m) \cdot (k+1)} - (-1)^{s(m) \cdot k}| &= \frac{1}{2} \sum_{k=0}^{\frac{M}{2}-2} |(-1)^{s(m) \cdot (\frac{M}{2}+k+1)} - (-1)^{s(m) \cdot (\frac{M}{2}+k)}| \\ &= \frac{1}{2} \sum_{k=0}^{\frac{M}{2}-2} |(-1)^{s_{m-1}} \left((-1)^{s(m) \cdot (k+1)} - (-1)^{s(m) \cdot k} \right)| \\ &= \frac{1}{2} \sum_{k=0}^{\frac{M}{2}-2} |((-1)^{s(m) \cdot (k+1)} - (-1)^{s(m) \cdot k})|. \end{aligned} \quad (2.9)$$

From Eq. (2.7), Eq. (2.8) and Eq. (2.9) it follows that

$$\begin{aligned} Z_m(s(m)) &= \left(\sum_{k=0}^{\frac{M}{2}-2} |(-1)^{s(m) \cdot (k+1)} - (-1)^{s(m) \cdot k}| \right) + (s_0 \oplus s_1 \oplus \dots \oplus s_{m-1}) \\ &= \left(\sum_{k=0}^{\frac{M}{2}-2} |(-1)^{s(m-1) \cdot (k+1)} - (-1)^{s(m-1) \cdot k}| \right) + (s_0 \oplus s_1 \oplus \dots \oplus s_{m-1}). \end{aligned} \quad (2.10)$$

The last step follows because as k runs through 0 to $\frac{M}{2} - 2 = 2^{m-1} - 2$, the computations of $s(m) \cdot (k+1)$ and $s(m) \cdot k$ involve only the $m-1$ least significant bits of s , allowing one to write $s(m) \cdot (k+1) = s(m-1) \cdot (k+1)$ and $s(m) \cdot k = s(m-1) \cdot k$. Hence, we obtain

$$Z_m(s(m)) = 2Z_{m-1}(s(m-1)) + (s_0 \oplus s_1 \oplus s_2 \oplus \dots \oplus s_{m-1}),$$

and the proof is complete. \square

Corollary 2.1.2. *Let $s = s_{n-1} s_{n-2} \dots s_1 s_0$ with $s_j \in \{0, 1\}$. If $Z_n(s)$ is defined as*

$$Z_n(s) := \frac{1}{2} \sum_{k=0}^{2^n-2} |(-1)^{s \cdot (k+1)} - (-1)^{s \cdot k}|,$$

then

$$Z_n(s) = \sum_{k=0}^{n-1} g_k 2^k, \quad (2.11)$$

where $g_{n-1} = s_0$ and $g_k = s_0 \oplus s_1 \oplus \dots \oplus s_{n-1-k}$ for $k = n-2$ to $k = 0$.

Proof. It is easy to see from Eq. (2.6) that

$$\begin{aligned} Z_1(s(1)) &= s_0 = g_{n-1} \\ Z_2(s(2)) &= 2Z_1(s(1)) + (s_0 \oplus s_1) = 2g_{n-1} + g_{n-2} \\ Z_3(s(3)) &= 2Z_2(s(2)) + (s_0 \oplus s_1 \oplus s_2) = 2^2 g_{n-1} + 2g_{n-2} + g_{n-3}. \end{aligned}$$

A simple induction argument, whose details we skip, and the observation that $s(n) = s$ (see Sec. 1.1), shows that

$$Z_n(s) = \sum_{k=0}^{n-1} g_k 2^k.$$

This completes the proof. \square

Clearly, $Z_n(s)$ computes the number of zero-crossings of the sequence \mathcal{S} (ref. Eq. (2.1) and Eq. (2.2)). In the following, we give an example to illustrate the steps for computing $Z_n(s)$.

Example 2.1.3. Let $n = 3$ and $s = 5$ (or equivalently $s = 101$ as a binary string). We have

$$\mathcal{S} = ((-1)^{s \cdot 0}, (-1)^{s \cdot 1}, (-1)^{s \cdot 2}, \dots, (-1)^{s \cdot 7}) = (1, -1, 1, -1, -1, 1, -1, 1).$$

Let $N = 2^n = 8$. As $s = 101$, we have $s_0 = 1$, $s_1 = 0$ and $s_2 = 1$. The number of zero-crossings of the sequence \mathcal{S} is given by

$$Z_3(s) = Z_3(s(3)) = 2Z_2(s(2)) + (s_0 \oplus s_1 \oplus s_2) = 2Z_2(s(2)) + (1 \oplus 0 \oplus 1) = 2Z_2(s(2)). \quad (2.12)$$

We have, $s(2) = 01$. Therefore,

$$Z_2(s(2)) = 2Z_1(s(1)) + (s_0 \oplus s_1) = 2Z_1(s_0) + (1 \oplus 0) = 2(1) + 1 = 3. \quad (2.13)$$

From Eq. (2.12) and Eq. (2.13) we get $Z_3(s) = 6$, which is the same result that we obtained in Ex. 2.0.1.

3 Sequence ordered Walsh-Hadamard transforms

In this section, we will briefly recall the Walsh basis functions in seqency and natural ordering. We will also discuss the Walsh-Hadamard transforms in seqency and natural ordering and describe a quantum circuit for performing the Walsh-Hadamard transforms in seqency ordering. Interested readers may refer to [42] for further details on Walsh basis functions, Walsh-Hadamard transforms, and their applications.

3.1 Walsh basis functions in seqency and natural ordering

Walsh basis functions $W_k(x)$ for $k = 0, 1, 2, \dots, N-1$ in seqency order are defined as follows

$$W_0(x) = 1 \quad \text{for } 0 \leq x \leq 1, \quad (3.1)$$

$$W_{2k}(x) = W_k(2x) + (-1)^k W_k(2x-1), \quad (3.2)$$

$$W_{2k+1}(x) = W_k(2x) - (-1)^k W_k(2x-1), \quad (3.3)$$

$$W_k(x) = 0 \quad \text{for } x < 0 \text{ and } x > 1, \quad (3.4)$$

where N is an integer of the form $N = 2^n$. For $N = 8$ the Walsh functions in seqency order are shown in Fig. 1.

The number of sign changes (or zero-crossings) for the Walsh functions increases as the orders of the functions increase. A vector of length N can be obtained by sampling a Walsh basis function. The Walsh-Hadamard transform matrix in seqency order is obtained by arranging the vectors obtained from sampling

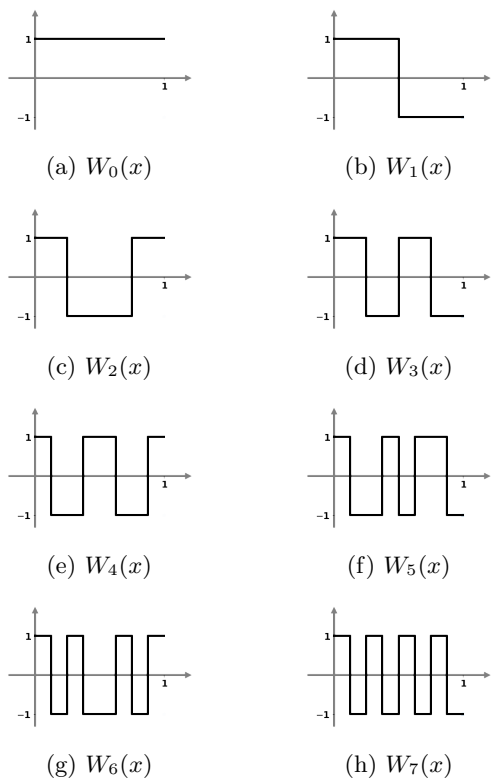


Figure 1: Walsh basis functions in the sequency ordering for $N = 8$.

the Walsh basis functions as the rows of a matrix. The vectors are arranged in increasing order of sequency. The Walsh-Hadamard transform matrix of order $N = 8$ in sequency order is

$$\frac{1}{\sqrt{8}} \begin{pmatrix} 1 & 1 & 1 & 1 & 1 & 1 & 1 & 1 \\ 1 & 1 & 1 & 1 & -1 & -1 & -1 & -1 \\ 1 & 1 & -1 & -1 & -1 & -1 & 1 & 1 \\ 1 & 1 & -1 & -1 & 1 & 1 & -1 & -1 \\ 1 & -1 & -1 & 1 & 1 & -1 & -1 & 1 \\ 1 & -1 & -1 & 1 & -1 & 1 & 1 & -1 \\ 1 & -1 & 1 & -1 & -1 & 1 & -1 & 1 \\ 1 & -1 & 1 & -1 & 1 & -1 & 1 & -1 \end{pmatrix}.$$

In contrast, the Walsh-Hadamard transform matrix of order $N = 2^n$ in natural order is given by

$$H_N = H^{\otimes n},$$

where

$$H = \frac{1}{\sqrt{2}} \begin{pmatrix} 1 & 1 \\ 1 & -1 \end{pmatrix}.$$

and $N = 2^n$. The Walsh-Hadamard matrix in natural order for $N = 8$ is

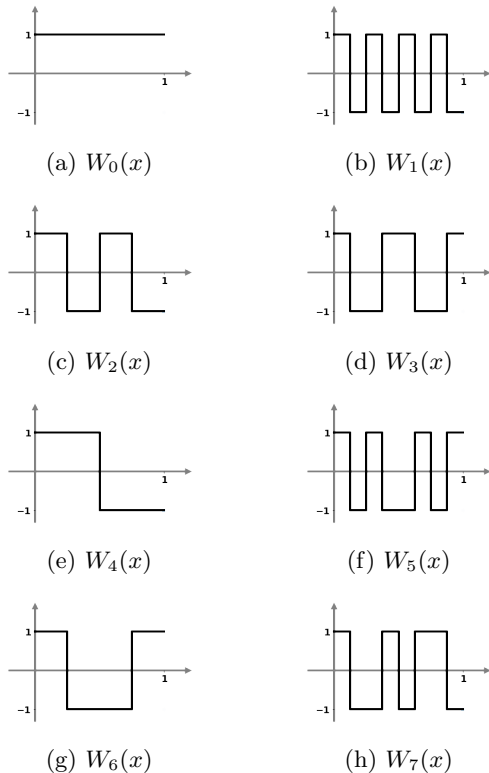


Figure 2: Walsh basis functions in the natural ordering for $N = 8$.

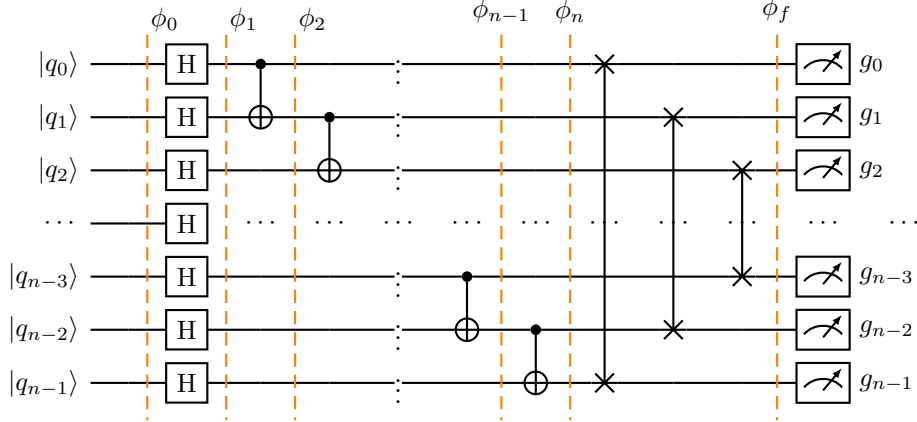


Figure 3: Quantum circuit for computing the Walsh-Hadamard transform in seqency ordering.

$$\frac{1}{\sqrt{8}} \begin{pmatrix} 1 & 1 & 1 & 1 & 1 & 1 & 1 & 1 \\ 1 & -1 & 1 & -1 & 1 & -1 & 1 & -1 \\ 1 & 1 & -1 & -1 & 1 & 1 & -1 & -1 \\ 1 & -1 & -1 & 1 & 1 & -1 & -1 & 1 \\ 1 & 1 & 1 & 1 & -1 & -1 & -1 & -1 \\ 1 & -1 & 1 & -1 & -1 & 1 & -1 & 1 \\ 1 & 1 & -1 & -1 & -1 & -1 & 1 & 1 \\ 1 & -1 & -1 & 1 & -1 & 1 & 1 & -1 \end{pmatrix}.$$

Walsh basis functions (or Hadamard-Walsh basis functions) in natural order can be obtained using the rows of the Walsh-Hadamard matrix H_N . For $N = 8$, the Walsh functions in natural order are shown in Fig. 2.

The Walsh-Hadamard transforms in natural and seqency orders can also be defined in terms of their actions on the computational basis vectors. Let $N = 2^n$ be a positive integer. Let V be the N dimensional complex vector space generated by the computational basis states $\{|0\rangle, |1\rangle, \dots, |N-1\rangle\}$. We note that the Walsh-Hadamard transform in natural order can be defined as a linear transformation $H_N : V \rightarrow V$ such that the action of $H_N = H^{\otimes n}$ on the computational basis state $|j\rangle$, with $0 \leq j \leq N-1$ is given by

$$H_N |j\rangle = \frac{1}{\sqrt{N}} \sum_{k=0}^{N-1} (-1)^{k \cdot j} |k\rangle. \quad (3.5)$$

Here $k \cdot j$ denotes bit-wise dot product of k and j .

Next, we note that the Walsh-Hadamard transform in seqency order can be defined as a linear transformation $H_S : V \rightarrow V$ acting on the basis state $|j\rangle$, with $0 \leq j \leq N-1$, as follows (see [42]).

$$H_S |j\rangle = \frac{1}{\sqrt{N}} \sum_{k=0}^{N-1} (-1)^{\sum_{r=0}^{n-1} k_{n-1-r} (j_r \oplus j_{r+1})} |k\rangle, \quad (3.6)$$

where $k = k_{n-1} k_{n-2} \dots k_1 k_0$ and $j = j_{n-1} j_{n-2} \dots j_1 j_0$, are binary representations of k and j respectively, with $k_i, j_i \in \{0, 1\}$ for $i = 0, 1, \dots, n-1$, and $j_n = 0$.

3.2 Quantum circuit for performing the sequency ordered Walsh-Hadamard transforms

A schematic quantum circuit for performing the Walsh-Hadamard transform in sequency order is shown. In order to show that the quantum circuit in Fig. 3 computes the Walsh-Hadamard transforms in sequency ordering, we will compute the output when the input is a computational basis state $|\phi_0\rangle = |j\rangle$, with $0 \leq j \leq N-1$ and $N = 2^n$. We have

$$\begin{aligned} |\phi_1\rangle &= H^{\otimes n} |\phi_0\rangle = \frac{1}{\sqrt{N}} \sum_{s=0}^{N-1} (-1)^{j \cdot s} |s\rangle, \\ &= \frac{1}{\sqrt{N}} \sum_{s=0}^{N-1} (-1)^{\sum_{k=0}^{n-1} j_k s_k} |s\rangle. \end{aligned} \quad (3.7)$$

Similar to our discussion in Sec. 2.1, the remaining part of the circuit acts on $|s\rangle$ to give $|g\rangle$, where $g = \sum_{k=0}^{n-1} g_k 2^k$ and $g_{n-1} = s_0$, $g_k = s_0 \oplus s_1 \oplus \dots \oplus s_{n-1-k}$, for $k = n-2, \dots, 1, 0$ (see Eq. (2.4) and Eq. (2.3)). Further, it is easy to see that

$$s_k = g_{n-k} \oplus g_{n-k-1}, \quad k = 0, 1, \dots, n-1, \quad (3.8)$$

where it is assumed that $g_n = 0$. Also, the map sending $|s\rangle$ to $|g\rangle$ defined in (see Eq. (2.4) and Eq. (2.3)) is invertible. It can be easily checked and it also follows from the fact that the transformation that sends $|s\rangle$ to $|g\rangle$ is implemented by unitary quantum gates. Therefore, the summation that runs through $s = 0$ to $s = N-1$ in Eq. (3.7) can be replaced by the summation running through $g = 0$ to $g = N-1$. It follows that

$$\begin{aligned} |\phi_f\rangle &= \frac{1}{\sqrt{N}} \sum_{g=0}^{N-1} (-1)^{\sum_{k=0}^{n-1} j_k (g_{n-k} \oplus g_{n-k-1})} |g\rangle \\ &= \frac{1}{\sqrt{N}} \sum_{g=0}^{N-1} (-1)^{\sum_{r=0}^{n-1} j_{n-1-r} (g_r \oplus g_{r+1})} |g\rangle. \end{aligned} \quad (3.9)$$

From Eq. (3.6) and Eq. (3.9) it follows that the quantum circuit shown in Fig. 3 can be used for computing the Walsh-Hadamard transform in sequency order.

4 Quantum Algorithm for High-Sequency Noise Detection

In this section, we present a quantum algorithm designed to detect high-sequency noise components in quantum-encoded signals. Such components often correspond to rapid variations or abrupt transitions in the underlying classical signal, and their detection is vital in various applications, including signal processing, communication systems, and biomedical diagnostics. High-sequency noise, represented in the Walsh-Hadamard basis, is characterized by non-negligible amplitudes associated with high-sequency indices. These indices correspond to the number of zero-crossings in the respective Walsh functions. Our objective is to estimate the amplitude contribution of a specified high-sequency band in a given quantum state.

Given a normalized test signal encoded as a quantum state, our method applies a quantum circuit to perform a sequency-ordered Quantum Walsh-Hadamard Transform (QWHT), followed by a band-selective oracle that flags the presence of amplitudes in the target sequency range. Finally, depending on the in-

tended use of the algorithm, the flagged sequency-band information may either be retained coherently for further quantum processing or used to estimate the corresponding probability mass via quantum amplitude estimation.

4.1 Problem Statement

Let $N = 2^n$ denote the dimension of the Hilbert space for an n -qubit system. Given a normalized quantum state $|\psi_{\text{test}}\rangle$ representing a test signal, our goal is to estimate the probability mass $P_{[a,a+M)}$ in a specific high-sequency band defined by integers a and M such that $0 \leq a < a + M \leq N$. The target probability mass is given by:

$$P_{[a,a+M)} = \sum_{j=a}^{a+M-1} |\langle j | \psi_{\text{sequency}} \rangle|^2,$$

where $|\psi_{\text{sequency}}\rangle = \mathcal{W}|\psi_{\text{test}}\rangle$ denotes the sequency-domain representation obtained by applying the QWHT unitary \mathcal{W} .

4.2 Overall Algorithm Approach

The algorithm proceeds through three key stages. First, we transform the input state into the sequency basis by applying the QWHT, thereby aligning the state representation with Walsh basis functions ordered by sequency. Second, we apply a comparator-based oracle U_S that coherently marks basis states whose indices fall within the desired high-sequency band. Third, depending on a classical control flag, the algorithm either retains the resulting flagged quantum state for use as a subroutine within a larger quantum computation or applies quantum amplitude estimation to obtain a classical estimate of the probability mass associated with the flagged sequency band.

4.3 Detailed Oracle Design (U_S)

The oracle U_S marks computational basis states $|j\rangle$ lying in the sequency range $[a, a+M)$. This marking uses two quantum comparator circuits: one to test whether $j \geq a$, and another to test whether $j < a + M$. Each comparator uses a flag ancilla qubit to store the result of the inequality.

To check the lower bound, we apply a quantum comparator $C_{\geq}(Q, a)$ which flips a temporary ancilla Q_{temp1} to $|1\rangle$ if the index $j \geq a$. For the upper bound, we use $C_{<}(Q, a+M)$ to flip another ancilla Q_{temp2} to $|1\rangle$ if $j < a + M$. These two conditions are then combined via a Toffoli gate with Q_{temp1} and Q_{temp2} as controls and a primary flag qubit Q_{flag} as the target. This marks the main ancilla as $|1\rangle$ if and only if both conditions are satisfied.

To preserve unitarity, the comparators are then uncomputed, restoring Q_{temp1} and Q_{temp2} to $|0\rangle$. The oracle thus acts as:

$$U_S |i\rangle |0\rangle_{\text{flag}} = \begin{cases} |i\rangle |1\rangle_{\text{flag}} & \text{if } a \leq i < a + M \\ |i\rangle |0\rangle_{\text{flag}} & \text{otherwise} \end{cases}$$

This operation coherently encodes membership in the target sequency band into the flag qubit and may be used either as a control for subsequent quantum operations or as the input to a quantum amplitude estimation routine. In Algorithm 1, this behavior is controlled by the classical Boolean flag `ESTIMATE`.

4.4 Amplitude Estimation for Probability Mass

This step is executed only when a classical estimate of the sequency-band probability mass is required. After applying the oracle U_S to the sequency-transformed state $|\psi_{\text{sequency}}\rangle|0\rangle_{\text{flag}}$, the overall system evolves as:

$$U_S |\psi_{\text{sequency}}\rangle|0\rangle_{\text{flag}} = \sum_{j=a}^{a+M-1} \langle j|\psi_{\text{sequency}}\rangle|j\rangle|1\rangle_{\text{flag}} + \sum_{j \notin [a, a+M]} \langle j|\psi_{\text{sequency}}\rangle|j\rangle|0\rangle_{\text{flag}}.$$

The probability of measuring the flag qubit Q_{flag} in state $|1\rangle$ is equal to the sum of squared amplitudes in the target band:

$$\Pr(Q_{\text{flag}} = 1) = \sum_{j=a}^{a+M-1} |\langle j|\psi_{\text{sequency}}\rangle|^2 = P_{[a, a+M]}. \quad (4.1)$$

Using QAE, we estimate this quantity efficiently. The final output of the algorithm is an estimate $P_{\text{est}} \approx P_{[a, a+M]}$, representing the total probability mass of the specified high-sequency components in the input signal.

Algorithm 1: Quantum algorithm for the detection of sequency-band structure

Input: A normalized quantum state $|\psi_{\text{test}}\rangle$ on n qubits, stored in quantum register Q ; Integer $a \in [0, 2^n - 1]$ (starting sequency index); Integer $M \in [1, 2^n - a]$ (number of consecutive sequency states); Boolean flag $\text{ESTIMATE} \in \{\text{true}, \text{false}\}$.

Output: If $\text{ESTIMATE} = \text{false}$: flag qubit Q_{flag} marking sequency-band membership;
If $\text{ESTIMATE} = \text{true}$: classical estimate P_{est} of the probability mass in $[a, a + M]$.

/ Step 1: State preparation */*

1 Initialize the n -qubit register Q in state $|\psi_{\text{test}}\rangle$.

/ Step 2: Sequency-basis transformation via QWHT */*

2 Apply the sequency-ordered Quantum Walsh–Hadamard Transform (QWHT):

(i) Apply Hadamard gates H to each qubit in Q .

(ii) For $k = 0$ to $n - 2$, apply a CNOT gate from Q_k to Q_{k+1} , with control being Q_k and target Q_{k+1} .

(iii) Apply SWAP gates to reverse qubit order for correct sequency indexing.

/ Step 3: Sequency-band oracle U_S for $[a, a + M]$ */*

3 Introduce ancilla qubits:

- Flag qubit Q_{flag} initialized to $|0\rangle$,
- Temporary ancillas Q_{temp1} and Q_{temp2} initialized to $|0\rangle$.

Implement U_S as follows:

- Apply comparator $C_{\geq}(Q, a)$, setting $Q_{\text{temp1}} = 1$ iff $Q \geq a$.
- Apply comparator $C_{<}(Q, a + M)$, setting $Q_{\text{temp2}} = 1$ iff $Q < a + M$.
- Apply a Toffoli gate with controls $(Q_{\text{temp1}}, Q_{\text{temp2}})$ and target Q_{flag} .
- Uncompute Q_{temp2} using $C_{<}^{\dagger}(Q, a + M)$.
- Uncompute Q_{temp1} using $C_{\geq}^{\dagger}(Q, a)$.

Effect: (Ignoring temporary ancillas)

$$U_S |i\rangle |0\rangle_{\text{flag}} = \begin{cases} |i\rangle |1\rangle_{\text{flag}}, & i \in [a, a + M], \\ |i\rangle |0\rangle_{\text{flag}}, & \text{otherwise.} \end{cases}$$

if $\text{ESTIMATE} = \text{false}$ **then**

return Flag qubit Q_{flag} (coherent sequency-band indicator).

end

else

/ Step 4: Amplitude estimation (conditional) */*

4 Apply a suitable amplitude estimation algorithm (e.g., MLQAE [43] or AWQAE [13]) using: State preparation from Step 2, Oracle U_S from Step 3, and Flag qubit Q_{flag} .

5 Let P_{est} denote the estimated probability $\text{Pr}(Q_{\text{flag}} = 1)$.

6 **return** P_{est} .

end

Remark 4.4.1. *Step 4 (Amplitude Estimation) is optional and is included only when a classical estimate of the sequency-band probability mass is required. If the proposed procedure is used as a coherent subroutine within a larger quantum algorithm, the output of Step 3 may be retained in quantum form without performing amplitude estimation or measurement. In this case, the flag qubit Q_{flag} coherently encodes membership in the sequency band $[a, a + M)$ and can be used as a control or input for subsequent quantum operations, such as conditional unitaries, amplitude amplification, or further oracle calls.*

4.5 Computational Complexity

We now analyze the computational resources required by the proposed algorithm. Throughout this discussion, $N = 2^n$ denotes the size of the signal, while n is the number of qubits used to represent it.

The sequency-ordered Quantum Walsh–Hadamard Transform (QWHT) is implemented by applying a standard n -qubit Hadamard transform followed by a cascade of CNOT and SWAP gates that map the natural ordering to sequency ordering. This construction requires $O(n)$ Hadamard gates, $O(n)$ CNOT gates, and $O(n)$ SWAP gates, resulting in an overall circuit depth of $O(n)$ for the QWHT stage.

The oracle U_S consists of two integer comparator circuits acting on n -qubit registers, each requiring $O(n)$ quantum gates and $O(n)$ ancilla qubits. A Toffoli gate is used to combine the comparator outputs, and the ancilla registers are subsequently uncomputed to preserve reversibility. Consequently, the oracle has circuit depth $O(n)$ and requires $O(n)$ ancillary qubits.

Classically, detection of the sequency band may be performed deterministically by computing the full discrete Walsh–Hadamard Transform (DWHT) of a length- N signal. Using fast Walsh–Hadamard transform algorithms, this requires $O(N \log N) = O(n 2^n)$ time complexity.

When the quantum input state corresponding to a length- N signal can be prepared efficiently using $O(\text{poly}(n))$ quantum operations, the proposed algorithm offers a significant advantage for high-dimensional signals ($N \gg 1$) and moderate accuracy requirements. We emphasize that the claimed advantage applies to probabilistic estimation of sequency-band energy and relies on the assumption of efficient quantum state preparation.

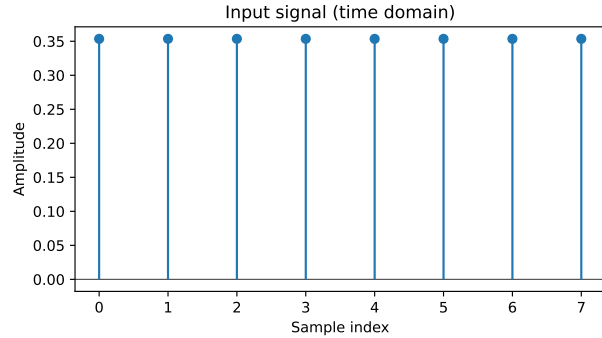
5 Numerical Simulations

This section presents numerical simulations validating the correctness of the proposed sequency-ordered Quantum Walsh–Hadamard Transform (QWHT) and the associated sequency band-energy estimation procedure. All simulations are performed using noiseless statevector evolution for small system sizes. The objective of these simulations is to verify consistency with the theoretical analysis.

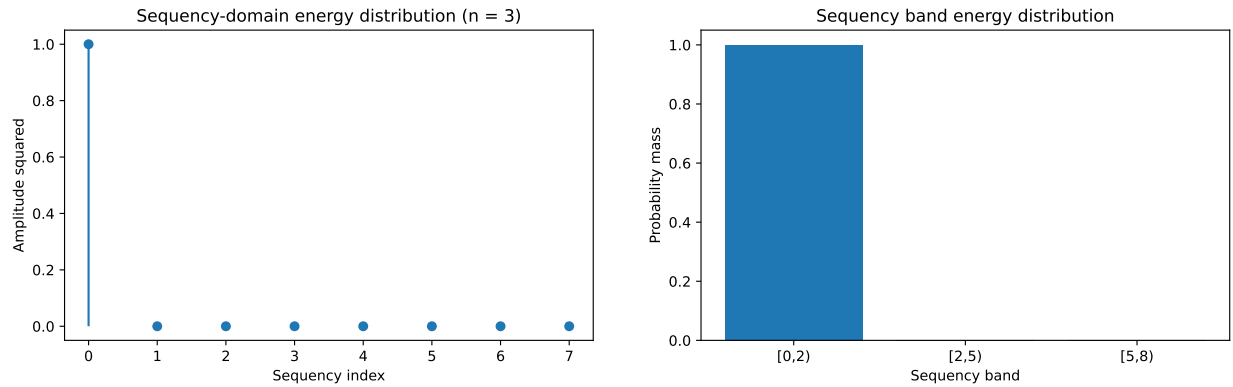
Unless stated otherwise, simulations are carried out for $n = 3$ data qubits, corresponding to $N = 2^n = 8$ computational basis states. This system size is sufficient to capture the essential features of the algorithm while allowing exact classical verification of all results. We consider several representative input signals, including smooth, low-sequency signals, highly oscillatory and structured-noise cases, to illustrate the behavior of the algorithm across different regimes.

Simulation methodology. For a real-valued input signal $\mathbf{x} = (x_0, x_1, \dots, x_{N-1})$, we prepare the normalized quantum state $|\psi_{\text{in}}\rangle = \sum_{j=0}^{N-1} x_j |j\rangle$, with $\sum_j |x_j|^2 = 1$. Applying the sequency-ordered QWHT yields the state $|\psi_{\text{seq}}\rangle = U_{\text{QWHT}} |\psi_{\text{in}}\rangle = \sum_{k=0}^{N-1} c_k |k\rangle$.

Due to the explicit Gray-code mapping and bit-reversal operations implemented in the circuit, the computational basis states $|k\rangle$ at the output of the QWHT correspond directly to sequency indices. The quantity



(a) Time-domain signal



(b) Sequencey spectrum

(c) Band-energy histogram

Figure 4: Numerical results for the constant (DC) input signal.

$|c_k|^2$ therefore represents the contribution of sequence index k to the total signal energy.

To validate the oracle-based band selection, the sequencey indices are partitioned into three disjoint bands $[0, b)$, $[b, b + M)$, and $[b + M, N)$. For the simulations that follow we have used $b = 2$ and $M = 3$. For any band $[u, v)$, the associated band energy is $P_{[u, v)} = \sum_{k=u}^{v-1} |c_k|^2$. This probability mass is exactly the quantity targeted by amplitude estimation in the full algorithm and is extracted directly from the statevector in the present simulations.

Constant (DC) input signal. Figure 4 shows the numerical results for a constant input signal. The time-domain plot confirms the absence of sign changes. The sequencey-domain spectrum exhibits a single nonzero component at the lowest sequence index, and the band-energy histogram shows that all probability mass is concentrated in the lowest sequence band.

Piecewise-constant (edge-like) input signal. Figure 5 presents the results for a piecewise-constant signal containing a single sharp transition. The time-domain plot highlights one sign change. The sequencey-domain spectrum shows energy distributed over low and intermediate sequence indices, while the band-energy histogram confirms that the probability mass is shared between the corresponding sequence bands.

Alternating-sign input signal. Figure 6 shows the results for an alternating-sign input signal. The time-domain plot exhibits the maximal number of sign changes. Correspondingly, the sequencey-domain spectrum is dominated by high-sequence components, and the band-energy histogram shows that most of the probability mass lies in the high-sequence band.

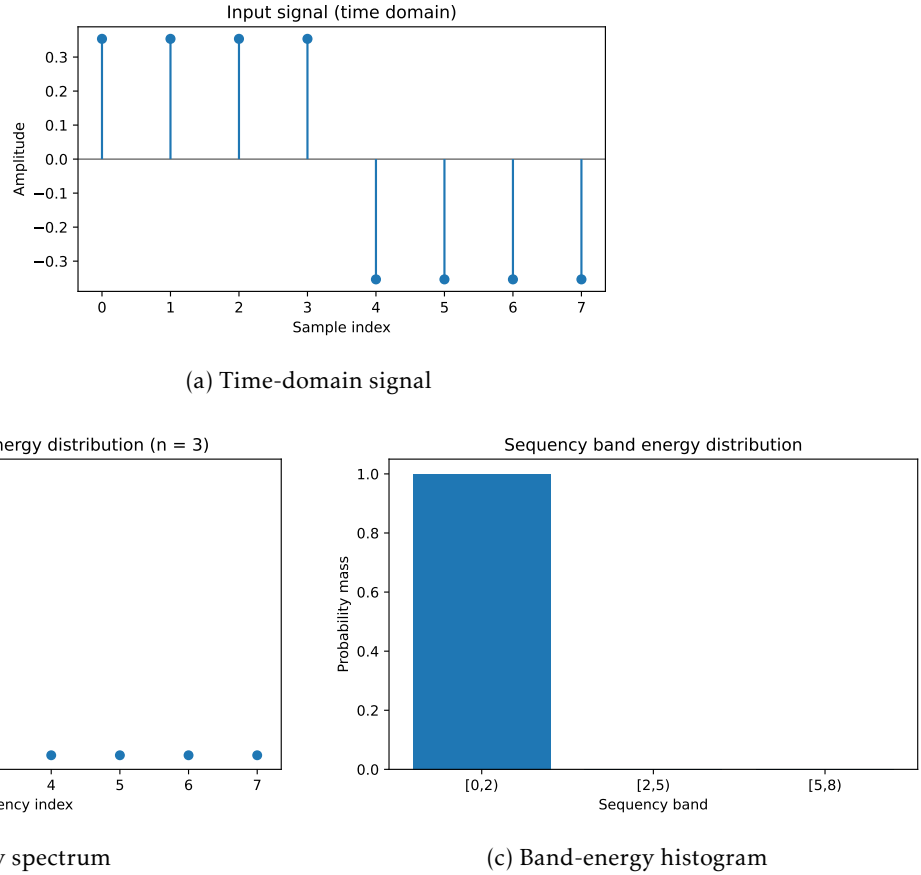


Figure 5: Numerical results for the piecewise-constant (edge-like) input signal.

Summary and Discussion. Across all tested signals, the numerical simulations show a consistent correspondence between time-domain structure, seqency-domain energy spectra, and seqency band-energy distributions. These results confirm that the proposed QWHT correctly implements seqency ordering, that computational basis states at the output can be interpreted directly as seqency indices, and that the oracle-based procedure accurately estimates aggregate seqency band energy.

Beyond its role in estimating aggregate seqency content, the proposed band-energy estimation procedure admits a natural interpretation as a form of structure-based anomaly detection in the seqency domain. For a given class of nominal signals characterized by predominantly low-seqency structure, the appearance of significant probability mass in higher seqency bands indicates a deviation from the expected signal behavior. In this sense, high-seqency noise or rapid sign-change structure manifests as an anomaly that can be detected by monitoring the estimated band energies. We emphasize that the present work does not address learning-based, adaptive, or statistical anomaly detection, but rather provides a deterministic, oracle-based metric that is directly tied to the physical structure of the signal.

6 Conclusion

In this work, we introduced a fully quantum framework for seqency-resolved signal analysis based on the seqency-ordered Quantum Walsh–Hadamard Transform (QWHT). By combining a low-depth imple-

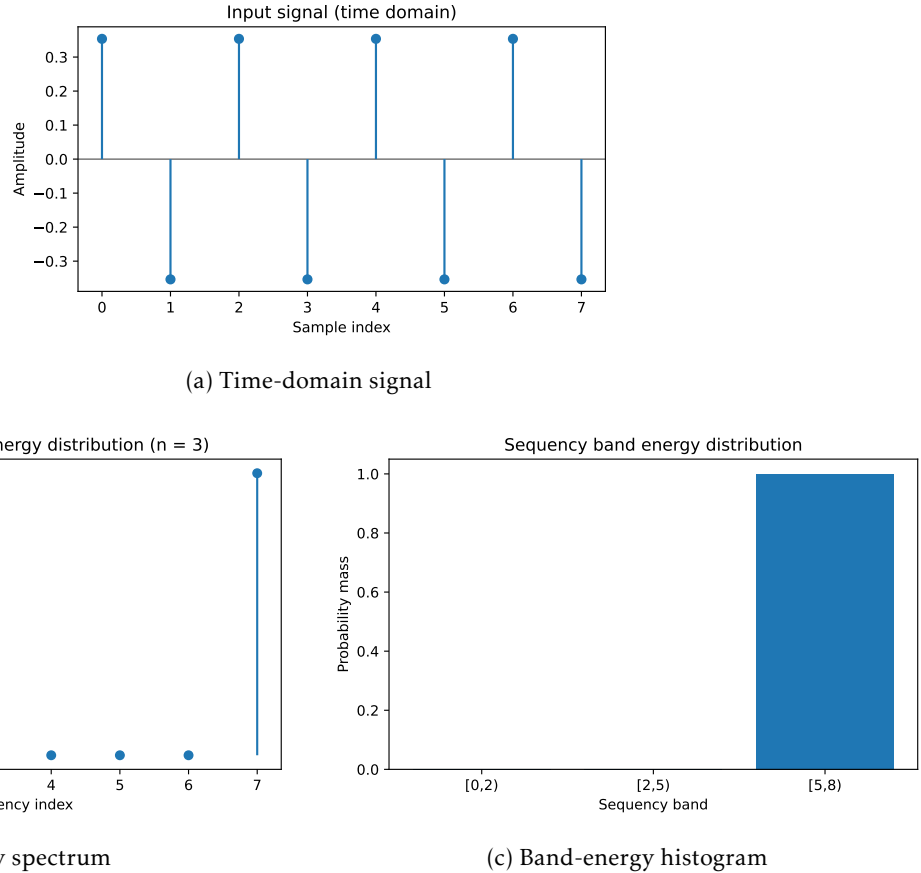


Figure 6: Numerical results for the alternating-sign input signal.

mentation of the QWHT with a comparator-based, coherently reversible sequency-band oracle, we showed how to isolate and quantify the contribution of user-specified sequency bands in quantum-encoded signals. When a classical estimate is required, the marked sequency information can be converted into a probability estimate using Quantum Amplitude Estimation (QAE); alternatively, the output may be retained coherently and used directly as a subroutine within a larger quantum algorithm.

A key outcome of this work is the demonstration that the sequency-ordered QWHT can be implemented with circuit depth $O(\log_2 N)$ (equivalently $O(n)$ for $N = 2^n$) on an amplitude-encoded quantum state. In contrast, classical approaches that explicitly compute the Walsh–Hadamard spectrum of a length- N signal require $O(N \log_2 N)$ operations. When the proposed method is embedded as a module within a larger quantum computation, so that both input and output remain quantum, this represents an exponential advantage.

From an application perspective, sequency-band energy estimation provides a structure-based indicator of rapid sign-change behavior, closely related to classical notions of zero-crossings and high-frequency noise. This makes the proposed algorithm relevant to quantum-enhanced signal processing tasks such as band-limited noise detection, edge and anomaly detection, and feature extraction in the Walsh basis. The numerical simulations presented for small system sizes confirm the correctness of the sequency ordering, the interpretation of output basis states as sequency indices, and the correspondence between time-domain structure and sequency-domain energy concentration.

Several directions remain open for future work. These include experimental realization on near-term quantum hardware, optimization of comparator and oracle circuits for noise-resilient implementations, and integration with variational or hybrid quantum-classical schemes for adaptive noise suppression and signal classification. More broadly, the techniques developed here, particularly sequency-ordered transforms and band-selective quantum oracles, provide a reusable primitive for structured spectral analysis within the growing landscape of quantum signal processing.

References

- [1] Michael A. Nielsen and Isaac Chuang. *Quantum Computation and Quantum Information*. Cambridge University Press, 2000.
- [2] David Deutsch and Richard Jozsa. Rapid solution of problems by quantum computation. *Proceedings of the Royal Society of London. Series A: Mathematical and Physical Sciences*, 439(1907):553–558, 1992.
- [3] Ethan Bernstein and Umesh Vazirani. Quantum complexity theory. In *Proceedings of the twenty-fifth annual ACM symposium on Theory of computing*, pages 11–20, 1993.
- [4] Alok Shukla and Prakash Vedula. A generalization of Bernstein–Vazirani algorithm with multiple secret keys and a probabilistic oracle. *Quantum Information Processing*, 22(6):244, 2023.
- [5] Daniel R Simon. On the power of quantum computation. *SIAM journal on computing*, 26(5):1474–1483, 1997.
- [6] Lov K Grover. A fast quantum mechanical algorithm for database search. In *Proceedings of the Twenty-eighth Annual ACM Symposium on Theory of Computing*, pages 212–219. ACM, 1996.
- [7] Alok Shukla and Prakash Vedula. An efficient implementation of a quantum search algorithm for arbitrary n. *The European Physical Journal Plus*, 140(6):575, 2025.
- [8] A Yu Kitaev. Quantum measurements and the abelian stabilizer problem. *arXiv preprint quant-ph/9511026*, 1995.
- [9] Miroslav Dobšíček, Göran Johansson, Vitaly Shumeiko, and Göran Wendin. Arbitrary accuracy iterative quantum phase estimation algorithm using a single ancillary qubit: A two-qubit benchmark. *Physical Review A—Atomic, Molecular, and Optical Physics*, 76(3):030306, 2007.
- [10] Gilles Brassard, Peter Hoyer, Michele Mosca, and Alain Tapp. Quantum amplitude amplification and estimation. *Contemporary Mathematics*, 305:53–74, 2002.
- [11] Alok Shukla and Prakash Vedula. Towards practical quantum phase estimation: A modular, scalable, and adaptive approach. *arXiv preprint arXiv:2507.22460*, 2025.
- [12] Tudor Giurgica-Tiron, Iordanis Kerenidis, Farrokh Labib, Anupam Prakash, and William Zeng. Low depth algorithms for quantum amplitude estimation. *Quantum*, 6:745, 2022.
- [13] Alok Shukla and Prakash Vedula. Modular quantum amplitude estimation: A scalable and adaptive framework. *arXiv preprint arXiv:2508.05805*, 2025.

[14] Peter W Shor. Polynomial-time algorithms for prime factorization and discrete logarithms on a quantum computer. *SIAM review*, 41(2):303–332, 1999.

[15] Alok Shukla and Prakash Vedula. A modular, adaptive, and scalable quantum factoring algorithm. *arXiv preprint arXiv:2509.05010*, 2025.

[16] Alok Shukla and Prakash Vedula. Trajectory optimization using quantum computing. *Journal of Global Optimization*, 75(1):199–225, 2019.

[17] Aram W Harrow, Avinatan Hassidim, and Seth Lloyd. Quantum algorithm for linear systems of equations. *Physical Review Letters*, 103(15):150502, 2009.

[18] Andrew M Childs and Jin-Peng Liu. Quantum spectral methods for differential equations. *Communications in Mathematical Physics*, 375(2):1427–1457, 2020.

[19] Dominic W Berry. High-order quantum algorithm for solving linear differential equations. *Journal of Physics A: Mathematical and Theoretical*, 47(10):105301, 2014.

[20] Alok Shukla and Prakash Vedula. A hybrid classical-quantum algorithm for solution of nonlinear ordinary differential equations. *Applied Mathematics and Computation*, 442:127708, 2023.

[21] Alok Shukla and Prakash Vedula. A hybrid classical-quantum algorithm for digital image processing. *Quantum Information Processing*, 22(1):1–19, 2023.

[22] Alok Shukla and Prakash Vedula. A quantum approach for digital signal processing. *The European Physical Journal Plus*, 138(12):1–24, 2023.

[23] Mohit Rohida, Alok Shukla, and Prakash Vedula. Hybrid classical-quantum image processing via polar walsh basis functions. *Quantum Machine Intelligence*, 6(2):72, 2024.

[24] Mohit Rohida, Alok Shukla, and Prakash Vedula. Quantum algorithm for edge detection in digital grayscale images. *arXiv preprint arXiv:2507.06642*, 2025.

[25] Niels Gleinig and Torsten Hoefler. An efficient algorithm for sparse quantum state preparation. In *2021 58th ACM/IEEE Design Automation Conference (DAC)*, pages 433–438. IEEE, 2021.

[26] Fereshte Mozafari, Mathias Soeken, Heinz Riener, and Giovanni De Micheli. Automatic uniform quantum state preparation using decision diagrams. In *2020 IEEE 50th International Symposium on Multiple-Valued Logic (ISMVL)*, pages 170–175. IEEE, 2020.

[27] Alok Shukla and Prakash Vedula. An efficient quantum algorithm for preparation of uniform quantum superposition states. *Quantum Information Processing*, 23(2):38, 2024.

[28] Matthias Rosenkranz, Eric Brunner, Gabriel Marin-Sanchez, Nathan Fitzpatrick, Silas Dilkes, Yao Tang, Yuta Kikuchi, and Marcello Benedetti. Quantum state preparation for multivariate functions. *Quantum*, 9:1703, 2025.

[29] Hirmay Sandesara, Alok Shukla, and Prakash Vedula. A quantum approach for optimal control. *Quantum Inf Process* 24, 95 (2025), 2024.

[30] Naoharu H Shimada and Toshiya Hachisuka. Quantum coin method for numerical integration. In *Computer graphics forum*, volume 39, pages 243–257. Wiley Online Library, 2020.

- [31] Daniel S Abrams and Colin P Williams. Fast quantum algorithms for numerical integrals and stochastic processes. [arXiv preprint quant-ph/9908083](#), 1999.
- [32] Alok Shukla and Prakash Vedula. Efficient quantum algorithm for weighted partial sums and numerical integration. [Advanced Quantum Technologies](#), page e2500084, 2025.
- [33] WS Kuklinski. Fast Walsh transform data-compression algorithm: ECG applications. [Medical and Biological Engineering and Computing](#), 21(4):465–472, 1983.
- [34] C Zarowski and Maurice Yunik. Spectral filtering using the fast Walsh transform. [IEEE transactions on acoustics, speech, and signal processing](#), 33(5):1246–1252, 1985.
- [35] Yi Lu and Yvo Desmedt. Walsh transforms and cryptographic applications in bias computing. [Cryptography and Communications](#), 8(3):435–453, 2016.
- [36] Tom Beer. Walsh transforms. [American Journal of Physics](#), 49(5):466–472, 1981.
- [37] Henry F Ahner. Walsh functions and the solution of nonlinear differential equations. [American Journal of Physics](#), 56(7):628–633, 1988.
- [38] Peter A Gnoffo. Global series solutions of nonlinear differential equations with shocks using Walsh functions. [Journal of Computational physics](#), 258:650–688, 2014.
- [39] Peter A Gnoffo. Unsteady solutions of non-linear differential equations using Walsh function series. In [22nd AIAA Computational Fluid Dynamics Conference](#), page 2756, 2015.
- [40] Peter A Gnoffo. Solutions of nonlinear differential equations with feature detection using fast Walsh transforms. [Journal of Computational Physics](#), 338:620–649, 2017.
- [41] Alok Shukla. A quantum algorithm for counting zero-crossings. [arXiv preprint arXiv:2212.11814](#), 2022.
- [42] Kenneth George Beauchamp. [Walsh functions and their applications](#). Academic Press, 1975.
- [43] Yohichi Suzuki, Shumpei Uno, Rudy Raymond, Tomoki Tanaka, Tamiya Onodera, and Naoki Yamamoto. Amplitude estimation without phase estimation. [Quantum Information Processing](#), 19(2):1–17, 2020.